Comparative geometry of the San Andreas fault, California, and laboratory fault zones

D. E. MOORE
J. D. BYERLEE } *U.S. Geological Survey, Menlo Park, California 94025*

ABSTRACT

Textural examination of fault gouge deformed in triaxial friction experiments has revealed differences in the orientations of secondary shear sets between the stably sliding and stick-slip samples. In order to determine whether such differences can be identified in natural faults, maps of recently active breaks along the San Andreas fault from Point Arena to Cajon Pass, California, were examined to compare the types and orientations of secondary structures mapped in the creeping and locked sections. The fault zone was divided into 52 geometrically defined segments of uniform strike, which were then grouped into 7 sections: 4 straight and 2 curved sections, and Cholame Valley. One of the straight sections is the creeping section between San Juan Bautista and Cholame in central California; the rest of the sections are locked. Many of the gross geometric characteristics of the individual segments, such as length, width, and stepover size, reflect their position in either a straight or a curved section. In contrast, with respect to the orientations of the recent breaks within the segments, the single creeping section differs from all of the locked sections, both straight and curved, as follows: (1) the traces of recent breaks with a more westward orientation than the local strike of the fault zone (P traces) dominate over those with a more northward orientation (R traces) in the creeping section, whereas the opposite relationship holds in the locked sections, and (2) the more northward-oriented (R) traces make larger angles to the local strike of the fault zone in the locked sections than in the creeping section. The latter result is consistent with the orientations of R shears in our various laboratory samples. The former result was unexpected, because of the predominance of R shears in most laboratory samples, but a small number of samples are analogous to the creeping section in terms of their P-shear abundances, R-shear orientations, and sliding behavior. The causes of these distinguishing characteristics are not yet understood.

INTRODUCTION

A general correlation has long been made between the fracture patterns of natural fault zones and those that develop during laboratory shear box and friction tests (for example, Tchalenko, 1970; Wallace, 1973; Rutter and others, 1986). In recent years, we have conducted petrographic studies of fault gouge deformed in many triaxial friction experiments (Moore and others, 1986a, 1988, 1989). A major result of this work is that we have been able to distinguish between the stably sliding and stick-slip samples on the basis of the degree of development of subsidiary shears and their orientations relative to the boundaries of the gouge layers. We then wished to determine whether these experimental results could be applied to natural faults. To this end, we have studied the surface rupture patterns along the San Andreas fault zone, with emphasis on a comparison of the creeping and locked parts. This paper presents the first results of our study of San Andreas fault geometry and their evaluation in the light of our laboratory observations.

The analysis of fault geometry, and in particular fault segmentation, is becoming increasingly important because of the many recent demonstrations of correlations between earthquake rupture patterns and the locations of bends and stepovers along a fault (for example, Weaver and Hill, 1978; Bakun and others, 1980; Lindh and Boore, 1981; Sibson, 1985, 1986; Barka and Kadinsky-Cade, 1988). The geometric features identified in this investigation, therefore, may be applicable to the study of earthquake processes along the San Andreas fault zone.

EXPERIMENTAL BACKGROUND

The structural features produced during shear box, rotary shear, and Riedel experiments have been studied over many years (for example, Cloos, 1928; Riedel, 1929; Morgenstern and Tchalenko, 1967; Mandl and others, 1977), and investigators of rock mechanics have examined the fault patterns developed during friction experiments (for example, Logan and others, 1979, 1981; Rutter and others, 1986; Logan and Rauenzahn,

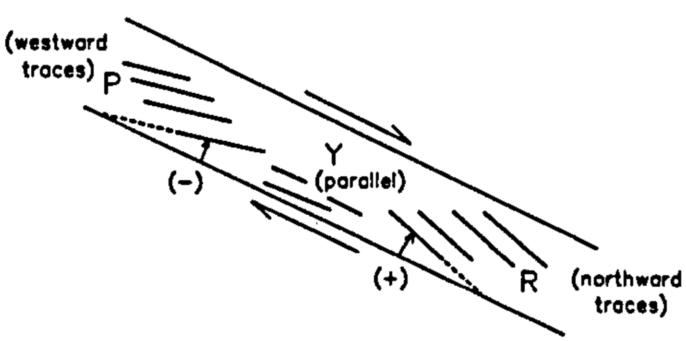

Figure 1. Labeling scheme and sign convention of Logan and others (1979) for selected secondary shears developed in gouge layers that were deformed in triaxial friction experiments. From comparison with our experimental results, the R and P shears make angles of at most ±35° to the boundaries of the fault zone. The fault zone is oriented with a northwest trend to compare with the northwest-trending, right-lateral San Andreas fault. In the discussion of San Andreas fault traces, those recent breaks making positive angles to the local fault strike, as indicated in the figure, are referred to as "northward" traces, and those making negative angles are termed "westward" traces.

Geological Society of America Bulletin, v. 103, p. 762–774, 9 figs., 3 tables, June 1991.

TABLE 1. CHARACTERISTICS OF GEOMETRICALLY DEFINED SEGMENTS OF THE SAN ANDREAS FAULT BETWEEN POINT ARENA AND CAJON PASS, CALIFORNIA

Segment	Average trend	Length (km)	Maximum width (m)	Nature of southeastern boundary
A-1	N31°W	9.2(+)	150	Gap (landslide and creek), modeled as simple bend (ocean on northwest side)
A-2	N36°W	34.3	990	Bend and offset; 75 m right step
A-3	N38°W	14.0	105	Bend and overlap; 150 m right step
A-4	N40°W	10.3	270	Bend and underlap; 270 m right step
A-5	N39°W	12.9(+)	310	Ocean
A-6	N35°W	22.0(+)	845	Bolinas Bay (bounded by Tomales Bay on northwest side)
B-1	N35°W	23.9(+)	505	Gap (reservoir); modeled as simple bend (ocean on northwest side)
B-2	N37°W	25.4	1,365	Simple bend
C-1	N48°W	8.8	730	Bend and overlap; 75 m right step
C-2	N42°W	8.2	305	Gap (creek and road), modeled as bend and offset; 135 m right step
C-3	N47°W	7.5	1,050	Bend and underlap; 440 m right step
C-4	N48°W	13.3	2,165	Bend and offset; 750 m *left* step
C-5a	N50°W	16.6	2,485	Underlap; 940m right step
C-5b	N50°W	5.2	1,750	Overlap; 365 m right step
C-5b′	N50°W	8.1	1,750	Bend and underlap; 480 m right step
C-6	N54°W	7.2	2,085	Simple bend
C-7	N47°W	11.4	1,635	Simple bend
C-8	N53°W	13.8	820	Simple bend
D-1	N47°W	12.1	350	Simple bend
D-2	N43°W	20.9	200	Bend and overlap; 150 m right step
D-3a	N40°W	20.5	410	Overlap; 250 m right step
D-3b	N40°W	26.3	635	Bend and underlap; 150 m right step
D-4	N42°W	66.0	1,385	Bend and underlap; 250 m right step
D-5a	N35°W	4.9	<50	Underlap; 750 m right step
D-5b	N35°W	8.2	<50	Simple bend
E-1	N41°W	29.0	655	Simple bend
E-2	N38°W	10.9	1,080	Bend and overlap; 325 m right step
E-3	N39°W	6.8	520	Bend and overlap; 150 m right step
E-4	N42°W	7.9	345	Gap (creek and road), modeled as bend and offset; 285 m right step
E-5	N41°W	18.3	240	Bend and overlap; 115 m right step
E-6	N43°W	10.4	185	Simple bend (smooth)
E-7	N48°W	6.9	1,135	Simple bend
E-8	N45°W	12.9	2,280	Simple bend
E-9a	N52°W	8.1	2,080	Underlap; 150 m right step
E-9b	N52°W	4.6	1,285	Bend and underlap; 420 m right step
E-10a	N56°W	8.4	1,990	Gap (hilly terrain), modeled as underlap; 170 m *left* step
E-10b	N56°W	5.7	205	Bend and underlap; 575 m *left* step
E-11	N68°W	9.6	345	Bend and offset; 95 m right step
E-12	N82°W	10.6	365	Gap (road), modeled as simple bend
E-13	N73°W	11.3	565	Gap (alluvium and road), modeled as simple bend
E-14	EW	4.8	420	Gap (road, alluvium, buildings), modeled as simple bend
E-15	N70°W	7.9	270	Gap (road), modeled as simple bend
F-1	N72°W	16.4	420	Simple bend
F-2	N71°W	20.6	535	Gap (alluvium and road), modeled as simple bend
F-3	N66°W	27.8	435	Gap (creeks and roads), modeled as simple bend
F-4	N65°W	10.6	1,630	Bend and overlap; 95 m right step
F-5a	N64°W	20.1	835	Offset; 90 m right step
F-5b	N64°W	9.1	260	Gap (creek and roads), modeled as simple bend
F-6a	N65°W	8.4	190	Overlap; 100 m right step
F-6b	N65°W	17.5	190	Gap (creek and roads), modeled as bend and underlap; 290 m right step
F-7	N60°W	14.0	190	Simple bend
F-8	N54°W	4.8(+)	<50	Southeast end of examined fault traces

1987). The laboratory experiments yield a variety of secondary shears oriented at different angles to the fault zone boundaries, along with tension fractures at about 45° to the principal direction of shear strain. Only three sets of shears, R, P, and Y, are important for this discussion (Fig. 1). The Y shears are approximately parallel to the strike of the fault zone, whereas the R and P shears make small to moderate angles of opposite sign (Fig. 1) to the trend of the fault zone. The sense of shear of all three sets of secondary shears is the same as that of the principal displacement zone.

The various types of laboratory faulting experiments cited above have yielded similar styles of fault zone evolution, which have been explained in terms of Coulomb theory (Morgenstern and Tchalenko, 1967; Tchalenko, 1970; Mandl and others, 1977; Naylor and others, 1986; Mandl, 1988; Sylvester, 1988). According to this theory, during standard simple-shear tests on materials such as sand and clay, the R shears form first as Coulomb shears. (The conjugate Coulomb shear, R′, would be oriented at about 60°–70° to the fault zone boundary; as a result, the conjugate Coulomb shears tend to be poorly developed.) The establishment of the R shears causes changes in the stress fields in the intervening areas, which in turn leads to the development of smaller-angle R shears, Y shears, and P shears in those areas. The original, larger-angle R shears are not well oriented to accommodate large amounts of slip, so that displacement gradually becomes more and more concentrated along the smaller-angle shears.

We have examined many samples of natural and simulated fault gouge that were deformed in laboratory triaxial friction experiments; the gouge materials tested include granitic rock flour, pure quartz sand, serpentine, and clay gouge rich in illite or montmorillonite (Moore and others, 1986a, 1988, 1989). The samples consisted of layers of gouge from 0.1 to 4.0 mm thick that were inserted along 30° sawcuts in granite cylinders. A maximum of about 15 mm offset along the sawcut was possible in the triaxial testing equipment. The friction experiments were run under a range of temperature, confining pressure, fluid pressure, and velocity conditions, which yielded many samples each of stable and stick-slip displacement (Summers and Byerlee, 1977; Byerlee and others, 1978; Moore and others, 1983, 1986a, 1986b).

In our samples that contained subsidiary shears, R and Y shears dominated, consistent with the other laboratory results; P shears were not uncommon, but with a few exceptions that are described later, their presence was restricted to short segments connecting other shears. The degree of localization of shear and the orientation of the R shears could be correlated with the sliding behavior of the samples. With respect to the illite-rich gouge (Moore and others, 1989), for which the most data are available, the samples with a pervasive deformation fabric and few or no subsidiary shears slid stably. The samples with deformation localized along subsidiary shears slid stably if the largest angle between the R shears and the boundary of the gouge layer (termed the "Riedel angle") was less than 10°, and stick-slip displacement occurred only if the maximum Riedel angle was larger than 14°. Samples with maximum Riedel angles between 10° and 14° had transitional behavior, that is, either stable slip, partially stable and partially stick-slip displacement, or stick-slip with small stress drops. The samples with the largest Riedel angles displayed the largest stress drops during the experiments. Similar relationships between gouge texture and sliding behavior were found in the other gouge types examined, although for the gouge composed of quartz sand, the R shears in the stably sliding samples made angles as large as 24° to the strike of the fault zone, and those in the stick-slip samples made angles of as much as 35° (Moore and others, 1988).

PRESENT STUDY

Scope

This work uses the six maps of recently active breaks along the San Andreas fault zone between Point Delgada and Cajon Pass, prepared at scales of 1:24,000 and 1:62,500 by geologists of the U.S. Geological Survey (Ross, 1969; Vedder and Wallace, 1970; Brown, 1970, 1972; Brown and Wolfe, 1972; Sarna-Wojcicki and others, 1975). A general view of this part of the San Andreas, with important locality names and the extent of each map, is presented in Figure 2. The study area north of San Francisco (Brown and Wolfe, 1972) was restricted to the on-land parts between Point Arena and Bolinas Bay. South of Cajon Pass, the San

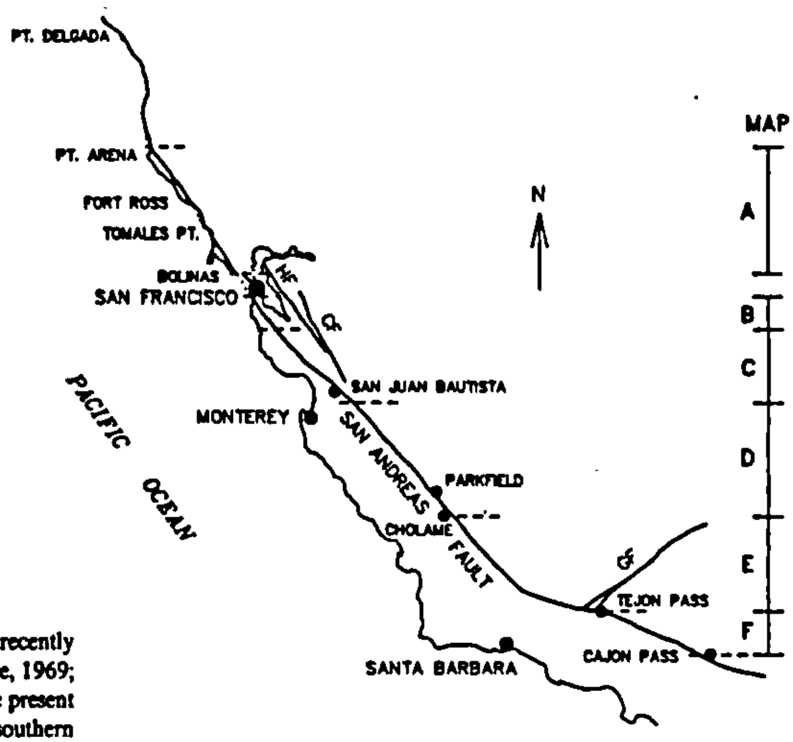

Figure 2. Map of the San Andreas fault between Point Arena and Cajon Pass; U.S. Geological Survey strip maps of recently active breaks along this part of the San Andreas are the focus of this study. The extent of each strip map is indicated by tick marks on the fault, which correspond to the map designations on the right: map A, Point Delgada to Bolinas Bay (Brown and Wolfe, 1972; only the part south of Point Arena has been examined); map B, San Mateo County (Brown, 1972); map C, Santa Cruz Mountains to northern Gabilan Range (Sarna-Wojcicki and others, 1975); map D, northern Gabilan Range to Cholame Valley (Brown, 1970); map E, Cholame Valley to Tejon Pass (Vedder and Wallace, 1970); map F, Tejon Pass to Cajon Pass (Ross, 1969). That part of the fault from just south of San Juan Bautista to near Cholame constitutes the creeping section of the San Andreas; the rest of the fault is locked. HF, Hayward fault; CF, Calaveras fault; GF, Garlock fault.

Andreas system splits into several major splays. Three maps of recently active fault traces have been compiled for parts of this area (Hope, 1969; Sharp, 1971; Clark, 1984), but they have been excluded from the present study because of the complicated nature of faulting in this part of southern California. They will be examined in the future, along with maps of the Hayward and Calaveras fault zones prepared by Radbruch-Hall (1974) and Herd (1977, 1978).

For this initial study, the data in the six maps were not modified with information from other sources, because the maps were prepared as part of the same project, with general guidelines set for the identification and depiction of the recent breaks. As a result, map-to-map variations arising from differences in mapping procedure should be minimized. Davis and Duebendorfer (1987) remapped the southeastern half of the area covered in Vedder and Wallace (1970); this map is considered separately to test the effect of differences in mapping technique on the results.

At a given locality, the San Andreas fault zone may consist of one or more individual fault traces—the recently active breaks—in a band as much as 2.5 km wide (Table 1). The recent breaks were identified by a combination of field and aerial-photograph examinations; because of inaccessibility or time constraints, not all of the features identified in the photographs were verified by field examinations. Topographic criteria for recent movement include scarps, trenches, offset streams, sag ponds, and lines of springs or trees (details of the mapping procedures are contained in the descriptions accompanying the maps). Many of these features are ephemeral, and their degree of preservation varies with climatic conditions, the rate of sedimentation or erosion, and the amount of human activity. Thus, the data set is probably incomplete, and some parts of the fault, such as arid regions, may yield a somewhat longer record of faulting than do others.

Procedures

The principal purpose of this study was to compare the orientations of the individual recent breaks to the local strike of the fault zone. Because the strike of the San Andreas varies markedly along its length (Fig. 2), we divided the fault zone into segments of uniform strike. Thus, the fault segments are defined solely on the basis of geometry, so that a given segment is a straight stretch of the fault zone that is separated from adjoining segments by geometric discontinuities such as bends or stepovers (Barka and Kadinsky-Cade, 1988; Knuepfer, 1989). Specifically, the length of a segment is the straight-line distance (the average trend or strike line) that can be traversed while remaining within the zone of recently active breaks. This usage differs from that of seismogenic or earthquake-rupture segments, which are defined on the basis of characteristic earthquakes that repeatedly rupture the same length of fault (Schwartz and Coppersmith, 1984).

The average trend line for a given segment was drawn as close as possible to the main trace of the fault zone, and segment boundaries were placed, where possible, at marked changes in the faulting pattern. Fault relations at several segment boundaries are concealed by recent alluvial deposits or construction. In such cases, the boundary was inferred. If projections of the average trend lines of the adjoining segments intersected within the gap, then the boundary was designated as a simple bend; otherwise, the smallest stepover width between the average trend lines in the gap was reported. Problems in defining segments were encountered

TABLE 2. GROUPING OF SAN ANDREAS FAULT SEGMENTS INTO STRAIGHT AND CURVED SECTIONS

Designation	Approximate trend	Segments	Average segment length (km)
(1) Northern locked section	N35°W	A-1 to B-2	17.7
(2) Northern curved section	N42°-54°W (range)	C-1 to C-7	9.6
(3) Central creeping section	N40°W	C-8 to D-4	26.6
(4) Cholame Valley	N35°W	D-5a to D-5b	6.5
(5) Central locked section	N40°W	E-1 to E-7	12.9
(6) Southern curved section	N45°-90°W (range)	E-8 to E-14	8.4
(7) Southern locked section	N65°W	E-15 to F-6b	15.4

principally in the complexly faulted parts of maps C and E, where the zone of rupturing is wide and the main fault trace is hard to identify. The southeastern half of map F near Cajon Pass was also problematic because, although the fault trend is not quite straight, the fault lacks obvious points of subdivision. Alternative divisions were examined for these parts of the fault; use of the alternative segment configurations does not affect the conclusions about comparative fault geometry reached in this paper. Measurements of fault-zone width were made along each segment, fault-zone width being defined in this study as the width of the zone of mapped recently active breaks, measured perpendicular to the strike line of the segment.

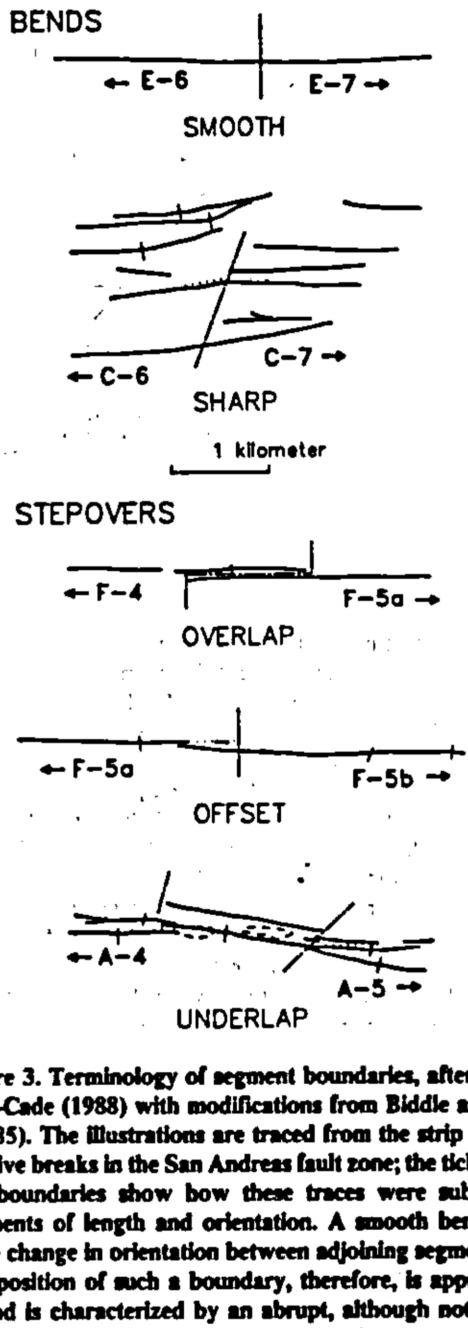

Figure 3. Terminology of segment boundaries, after Barka and Kadinsky-Cade (1988) with modifications from Biddle and Christie-Blick (1985). The illustrations are traced from the strip maps of recently active breaks in the San Andreas fault zone; the tick marks and segment boundaries show how these traces were subdivided for measurements of length and orientation. A smooth bend is one in which the change in orientation between adjoining segments is gradual. The position of such a boundary, therefore, is approximate. A sharp bend is characterized by an abrupt, although not necessarily large, change in the orientations of the recent breaks on either side of the boundary. The terminology of stepovers indicates the relationships along strike between adjoining segment ends. Dot-dashed lines mark the segment boundaries, and dotted lines in three of the sketches indicate the positions of the average trend lines. The dashed, closed lines in the area between segments A-4 and A-5 mark the sites of a swamp and a lake.

The strikes and lengths of all of the recent breaks within each segment were then measured. A small number of traces that appear to be landslide scars rather than fault ruptures were not considered. As in the case of the fault zone as a whole, the individual traces are seldom straight lines, and where necessary, they were divided into smaller lengths of relatively uniform trend. Subdividing rather than averaging was done, because the longer breaks, particularly the main fault trace, may have formed through the linkage of shorter, *en echelon* traces the orientations of which are the primary interest of this paper. Some examples of subdivided traces are shown in Figure 3. Subdivision of the traces is in many cases a subjective process because the changes in strike along a given fault trace are commonly gradual rather than abrupt. Efforts were made to ensure consistency in the manner of subdividing traces in the various maps. It should be kept in mind, however, that the rose diagrams and histograms of fault length and orientation and any numbers derived from them in this paper are to be considered in a comparative rather than an absolute sense.

Sets of the six maps containing the basic data for this report are available for inspection at five repository libraries, included with copies of Moore and Byerlee (1989). The maps show the exact positions of the segment boundaries and average trend lines, the subdivision of the individual fault traces for measurements of length and orientation, and the alternative segment boundaries that were considered. The locations of the libraries housing these maps are listed on page 19 of Moore and Byerlee (1989).

RESULTS

General Segment Characteristics

In all, 52 segments were defined along the examined 700 km of the San Andreas (Fig. 4 and Table 1), ranging from 4.6 to 66 km in length (Table 1) and averaging about 14 km. The average value is consistent with the 12- to 13-km-long, geometrically delimited segments of Bilham and Williams (1985) on the southern San Andreas and with the abundance of 12-km-long geometric segments defined by Bilham and King (1989) along the San Andreas between Cape Mendocino and the United States–Mexico border. All of the segments are less than 30 km long, except for one 66-km-long segment (D-4). Segment D-4 is on Brown's (1970) map, which was prepared at a 1:62,500 scale rather than the 1:24,000 scale used in most of the other strip maps. Irregularities in this segment may assume a greater prominence at the larger scale, leading to its division into smaller segments. As illustrated in Figure 5, the San Andreas is discontinuous at various scales, and moving from any given trace to the next closest one involves a change in strike or a stepover. The fault segments delimited in Figure 4 and Table 1 represent larger-scale discontinuities along the length of the zone of active faulting.

Among the segment boundaries, there are approximately equal numbers of simple bends and combined bends/stepovers, and a much smaller number of stepovers without bends. Unless otherwise noted, the bends listed in Table 1 are sharp bends (Fig. 3). The largest azimuthal difference between adjoining segments is 20°, measured between segments E-14 and E-15. Among the stepovers, overlaps and underlaps are more common designations than are offsets. All but three of the stepovers between segments are to the right. A right step on a right-lateral fault should be associated with extension (Crowell, 1974a, 1974b; Rodgers, 1980;

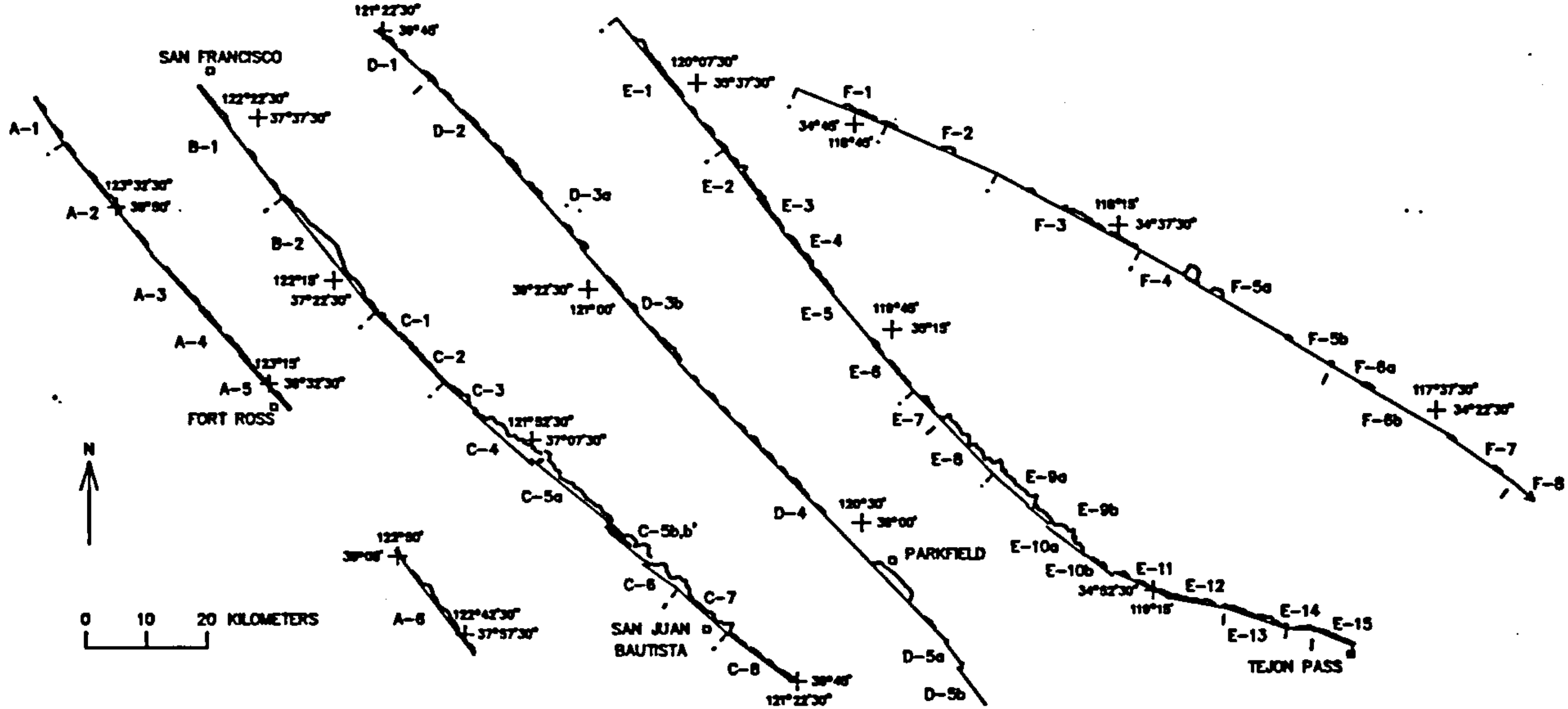

Figure 4. Schematic drawings of San Andreas fault segments and their inferred boundary relations. Gaps in the fault trace caused by alluvial deposits, road construction, and so on, are not shown. Segment boundaries not marked by stepovers are indicated by dashed lines. Each segment is represented by its average trend (strike) line; added to the upper side of each segment line are measurements of fault zone width, defined as the maximum distance between the mapped fault traces measured perpendicular to the average trend line. Therefore, the plotted widths do not reflect the actual distribution of recent breaks about the average trend lines. Length and width measurements are plotted at the same scale. Because of space limitations, the fault trace has been separated into pieces. Segment designations in the style of D-3a and D-3b represent adjoining segments with the same average trend that are separated by a stepover. Segments C-5b and C-5b' are segments that almost completely overlap. The edges of the strip maps are generally close to, but do not coincide with, segment boundaries.

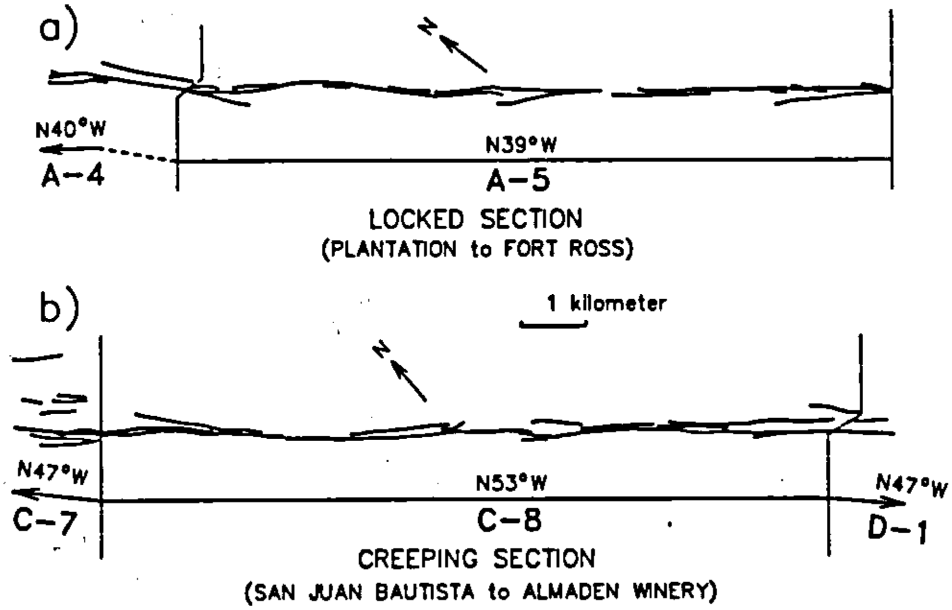

Figure 5. Tracings of representative segments from the (a) locked (A-5), and (b) creeping (C-8) parts of the San Andreas fault, with the average trend lines drawn directly beneath for reference. (On the original data maps of Moore and Byerlee, 1989, the average trend lines are drawn in the zone of recent breaks, to ensure that they are contained within the zone of active faulting and to facilitate the measurements of segment length and of bend and stepover size contained in Table 1.) Segment boundaries in the figures are indicated by dot-dashed lines.

Segall and Pollard, 1980; Sibson, 1985, 1986), and the boundary between segments A-4 and A-5 is a good illustration of this. The stepover area between these segments contains a lake and a swamp (Fig. 3), suggesting subsidence accompanying extension.

The maps examined in this study contain no information on the geological or structural relationships adjacent to the San Andreas fault zone. Comparison with the Davis and Duebendorfer (1987) map, however, which covers a 6-km-wide strip coincident with part of map E, shows that the segment boundaries delimited in that area are commonly located at the intersections of other faults with the San Andreas. At least some of our geometrically defined segments, therefore, also appear to have a structural significance.

Grouping of Segments into Sections

The strike of the San Andreas is relatively uniform over long stretches, but it changes markedly within a short distance along a major bend northwest of Tejon Pass (the western end of the Big Bend of many authors) and along a second, more subtle bend northwest of San Juan Bautista (the San Juan Bautista Bend of Crowell, 1979) (Fig. 2). The segments of these two bends differ in many of their characteristics from the segments in the more uniform stretches of fault, and we used these differences to devise an informal grouping of the segments into straight and curved sections (Fig. 6 and Table 2). The term "curved section" is used here instead of "bend," to avoid confusing these large-scale features with the bends between individual segments. In this study, the northern limit of section 2 (northern curved section) and the southern limit of section 6 (southern curved section) are placed at the sites of large azimuthal changes between adjoining segments (11° and 20°, respectively). The southern limit of section 2 and the northern limit of section 6 are situated at large, abrupt changes in fault-zone width (Fig. 4). The boundary between sections 2 and 3 also coincides with the southern termination of surface rupture accompanying the 1906 San Francisco earthquake and the northern limit of observed fault creep on the San Andreas.

The average segment length is about 17 km in the straight sections but only 8 km in the curved sections. The strike of adjoining segments in the straight sections tends to vary uniformly and gradually; the largest single bend is 6°. In contrast, the segments of the curved sections have a wide range of orientations, and the strike of adjoining segments tends to shift in a zig-zag (or sawtooth, Bilham and Williams, 1985) pattern. For example, between segments E-11 and E-15 in the southern curved section, the fault strike varies as follows: N68°W–N82°W–N73°W–N90°W–N70°W (Fig. 4, Table 1). The width of the zone of recent breaks is narrower overall in the straight sections, being in general less than 300 m and at most about 1,600 m in width (Fig. 4). The two parallel traces near Parkfield in the central creeping section are approximately 1,400 m apart. On the other hand, the maximum fault width is about 2,500 m in the northern curved section and 2,300 m in the southern one.

Cholame Valley consists of only two, parallel segments, and it does not correspond to either a straight or a curved section (Fig. 6 and Table 2). Nevertheless, it is the site of a pronounced discontinuity in the trend of the fault zone in central California, and it marks the southern end of the section of fault creep. Cholame Valley is generally viewed as a large, right stepover (Fig. 4; Dickinson, 1966; Sims, 1988; Shedlock and others, 1990); yet, because the main fault traces within the valley are of comparable length to the other segments in Table 1, it represents a higher-order stepover than those delimited between the individual segments and merits separate consideration.

Individual Fault Traces (Recently Active Breaks) in Segments

For each segment, the total length of fault traces with a given orientation was determined and plotted on a rose diagram (Fig. 7), to show the azimuthal range of the recently active fault traces. The rose diagrams vary widely from segment to segment, in part reflecting differences in segment length and density of faulting; even so, some trends can be seen. The diagrams with a narrow range of fault orientations are generally derived from segments of the straight sections. In contrast, the segments with a relatively wide range of fault orientations are concentrated in the curved sections. Nevertheless, within the entire study area, only two short traces are oriented more than 60° off the local average trend, and nearly 99% of the total fault length in Figure 7 is oriented within 35° of the local fault strike. The mode of fault length in a given rose diagram only rarely coincides with the average trend, instead diverging as much as 8° from it.

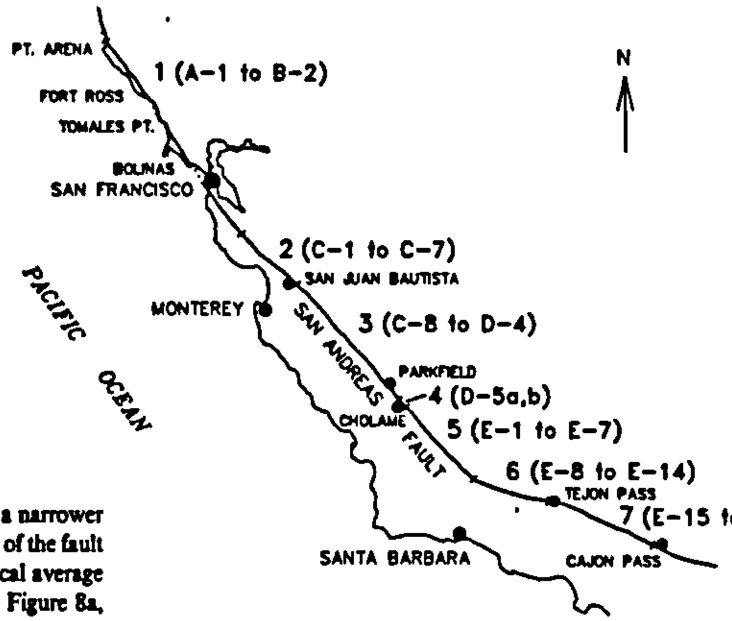

Figure 6. Grouping of the segments of the San Andreas fault into alternating straight and curved sections: 1, northern locked section; 2, northern curved section; 3, central creeping section; 4, Cholame Valley; 5, central locked section; 6, southern curved section; 7, southern locked section. General characteristics of the sections are listed in Table 2. Segments F-7 and F-8 are not included in the southern locked section (Table 2) because the strike of the fault changes by 11° along their 19-km combined length. These two segments may mark the beginning of a bend at the southern end of the study area.

The recent breaks of the creeping section are confined to a narrower angular range than are those of the locked sections (Fig. 8). All of the fault traces in the creeping section are oriented within 30° of the local average trend line. On the northward side shown in the histogram in Figure 8a, with the sole exception of two breaks at +26°, the fault traces make no more than a +15° angle to the local fault strike. Indeed, 97% of all of the fault traces in the creeping section are oriented within ±15° of the average trend. On the other hand, the histogram of the locked segments in Figure 8b tails off gradually to the 35° limits of the plots, and only 87% of the total fault length is contained in the range (+15° to –15°). If the shapes of the histograms in Figure 8 are compared, then the histogram for the creeping segments is skewed toward the westward (-) side, whereas that for the locked segments is skewed toward the northward (+) side. Expressed another way, for the creeping segments (Fig. 8a), the sum of the fault lengths for a given angle is generally greater on the westward side than on the northward side of the average trend; the opposite is true for the locked segments (Fig 8b). Comparison of the histograms in Figure 9 shows the concentration in the curved sections of fault traces making large angles to the average trend; nevertheless, such traces are also present in the locked straight sections. The histogram of the curved sections has less of a central peak than the one for the locked straight sections; both histograms, however, are skewed toward the northward side. Histograms for the individual segments (Moore and Byerlee, 1989) have more scatter, but the same overall trends are seen as described above for the grouped data.

TABLE 3. SEPARATION OF RECENT BREAKS INTO PARALLEL, NORTHWARD, AND WESTWARD FAULTS

	All creeping segments	All locked segments	Locked straight sections	Curved sections
Total measured length of recent breaks, L (km)	205.9	1123.4	517.4	577.4
Case 1: Range of parallel fault orientations, –1° to +1°				
Northward (km)	66.7	536.1	222.1	300.6
Parallel (km)	49.7	236.7	138.8	89.9
Westward (km)	89.4	350.7	156.4	187.7
$(\text{Westward/northward})_1$	1.34	0.65	0.70	0.62
$(\text{Parallel}/L)_1$	0.24	0.21	0.26	0.16
Case 2: Range of parallel fault orientations, –4° to +4°				
Northward (km)	39.4	359.1	119.1	228.7
Parallel (km)	112.5	544.6	307.6	220.3
Westward (km)	53.9	220.7	90.7	124.9
$(\text{Westward/northward})_2$	1.37	0.61	0.76	0.55
$(\text{Parallel}/L)_2$	0.55	0.48	0.58	0.38

The differences in the shapes of the histograms in Figures 8 and 9 are considered in more detail in Table 3, in which the fault lengths in the histograms are separated into three groups: those traces that are approximately parallel to the average trend, and those with either a more northward or a more westward orientation than the local fault strike. These groups are referred to as "parallel," "northward," and "westward," respectively. Six separate sets of calculations were made, for definitions of parallel faults ranging from 0° only (the average trend) to +5° to –5°; the results were almost the same for each case. Two of the intermediate sets of calculations are given in Table 3, as examples of relatively restricted (+1° to –1°) and relatively generous (–4° to +4°) definitions of the parallel faults, respectively; for each case, Table 3 lists the lengths of parallel, northward, and westward faults for the four groupings of segments in Figures 8 and 9. Because of the different total lengths of recent breaks in the histograms, two ratios were calculated to facilitate comparisons: the ratio of westward to northward faults, and the ratio of parallel faults to the total length of recent breaks in a given group of segments.

In both cases, the westward breaks dominate over the northward ones in the creeping section, whereas the opposite is true for the various groupings of locked segments (Table 3). The ratio of westward to northward traces is about 1.35 for the creeping segments and only 0.63 for all of the locked segments. These ratios differ by slightly more than a factor of 2; thus, relative to some unit length of northward traces, the creeping section contains more than twice the length of westward traces than do the locked sections. The ratio of westward to northward traces is higher for the locked straight sections than for the curved sections, but the former value still differs from the ratio for the creeping segments by a factor of 1.8 to 1.9. The proportion of parallel traces to the total length of recently active breaks is about the same for the creeping and the locked straight sections; for the narrower definition of parallel traces (case 1), the ratio is about 0.25 for both groups of segments, and for the wider definition of parallel breaks (case 2), the ratio is approximately 0.55 for both groups. The ratio of parallel traces to total fault length is lowest for the curved sections.

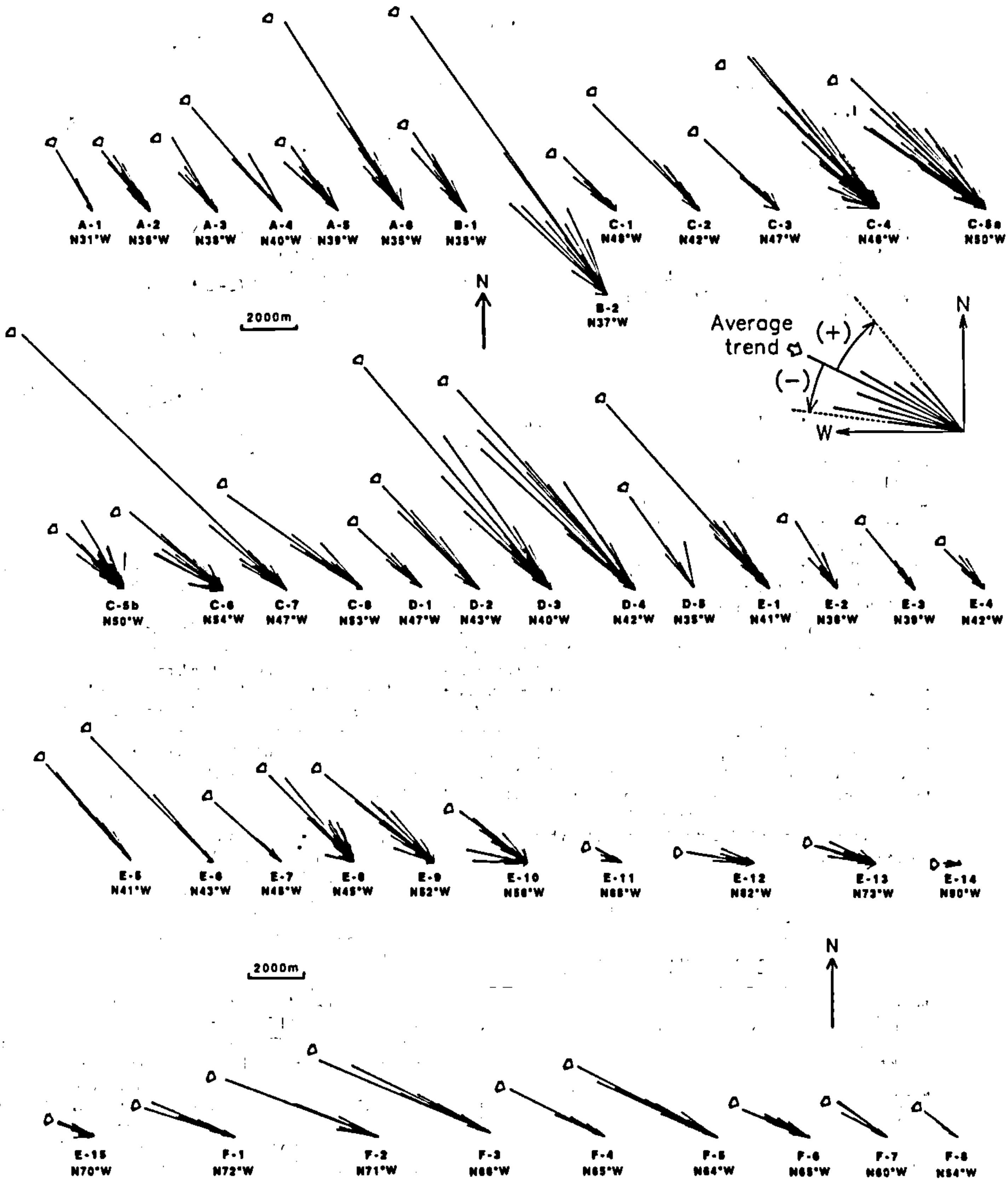

Figure 7. Rose diagrams of fault length relative to azimuthal position for the San Andreas fault segments. The average trend of each segment is indicated by an arrow. Adjoining segments with the same average trend have been grouped together with the exception of C-5a, which was kept separate from segments C-5b and C-5b′ because of the complexity of faulting in those segments.

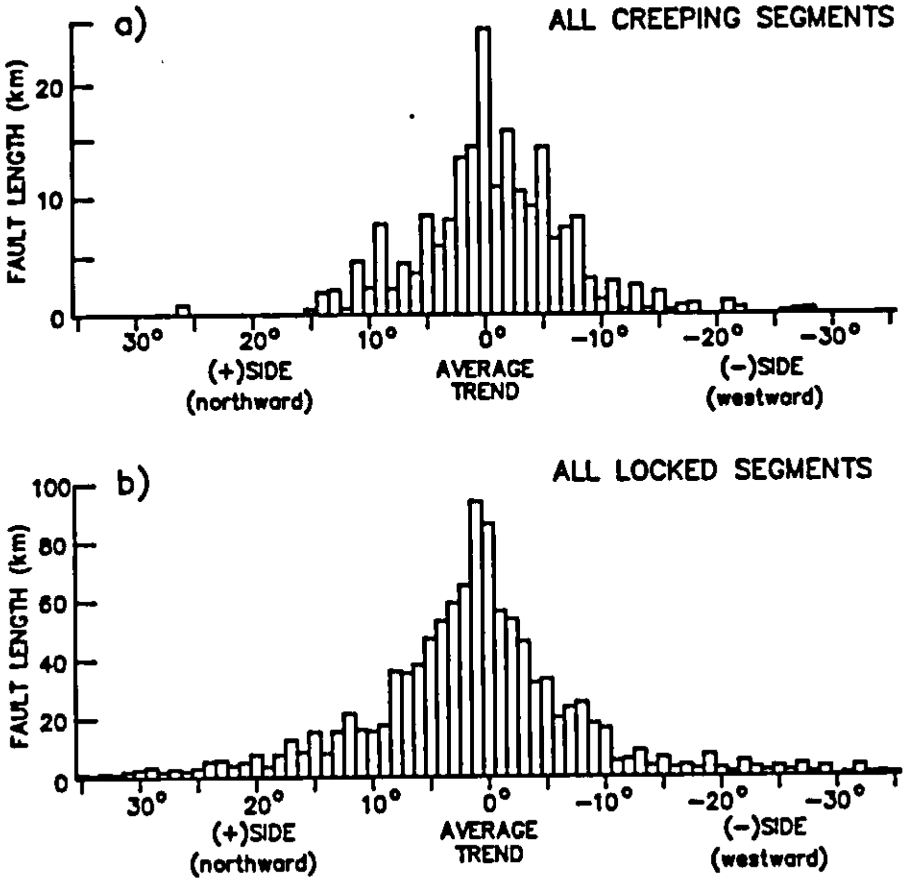

Figure 8. Histograms of the length of recently active breaks relative to the average trend for (a) all of the creeping segments and (b) all locked segments. Only those traces oriented within ±35° of the average trend are plotted; all of the recent breaks in the creeping segments but not all of those in the locked segments are in this range. The designation of (+) and (-) fault trace orientations is as illustrated in Figure 1. Histograms for the individual segments are presented in Moore and Byerlee (1989).

DISCUSSION

Comparison of Straight and Curved Sections

Several differences in the overall geometry of segments in the straight and curved sections of the San Andreas have been noted in this study. The curved sections are characterized by relatively short segments that are arranged in a sawtooth pattern. Both the stepovers and bends between adjoining segments tend to be larger in the curved sections, and the segments themselves occupy relatively wide and complex zones of faulting. These differences are consistent with the presence of an immature fault geometry in the curved sections and a more mature fault geometry in the straight sections. For example, Wesnousky (1988) proposed that the trace of a strike-slip fault becomes progressively more smooth with time. Wesnousky's index of smoothness was keyed to the number and sizes of stepovers; other logical consequences of progressive fault smoothing, however, would be the cutting off of high-angle bends and an increase in the average length of the fault segments.

The differences in fault patterns between the curved and straight sections cannot be ascribed to differences in their total ages and amounts of offset. Instead, the curved sections may be original features of the San Andreas that, because of tectonic constraints, were unable to straighten. A second possibility is that the curved sections originated through the recent bending of a formerly straight section of the fault, causing the fault patterns to become "reset." No conclusions can be drawn about the northern curved section at this time, because its tectonic history is not well understood (Aydin and Page, 1984). Crowell (1979) inferred, however, that this bend is a recent, superposed feature that is becoming more pronounced with time, with the relatively young Calaveras (Page, 1982) and Hayward faults developing as splay faults in response to the bending.

Two hypotheses have been advanced that may account for the presence of the southern curved section. Several workers have correlated the development of this large-scale bend with displacement on the Garlock fault. As summarized by Sylvester (1988), the modern San Andreas originated at about 24 Ma and has about 330 km right-lateral offset; the Garlock fault, which meets the San Andreas at the southeast end of the southern curved section (Fig. 2; see also Davis and Duebendorfer, 1987), has accumulated about 60 km left-lateral displacement since 10 Ma (Loomis and Burbank, 1988). The Garlock fault has been interpreted by Davis and Burchfiel (1973) as a continental transform fault that accommodates east-west, Basin and Range extension on the north side of the fault, with the relatively stable Mojave block on the south side. At the time of inception of the Garlock fault, the San Andreas of the southern curved section may have been straight and in line with the sections of the fault to the north and south of it (Bohannon and Howell, 1982); since then, progressive left-lateral offset on the Garlock fault has caused the San Andreas to be increasingly deflected to the west.

Alternatively, Crowell (1979) suggested that the San Gabriel fault was originally the main strand of the San Andreas in southern California. At about 4 Ma, perhaps in association with the opening of the Gulf of California, this strand was replaced by the current trace of the San Andreas between the Big Bend and the San Gorgonio Bend. The new trace would include both the southern curved and southern locked sections of this study. Comparison with the northern straight section, much of which originated in the past 4 m.y. (Atwater, 1970; Atwater and Molnar, 1973), suggests that a mature fault geometry, such as that exhibited by the south-

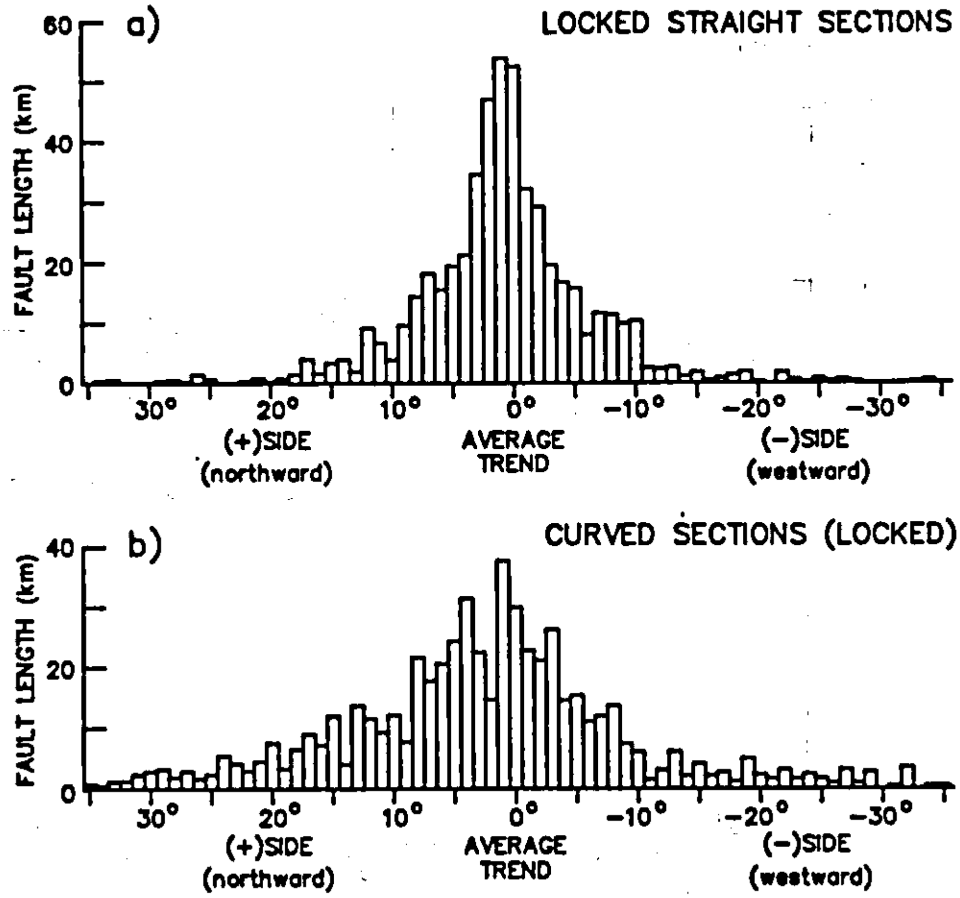

Figure 9. Histograms of fault trace length relative to the average trend for segments of (a) the locked straight sections (sections 1, 5, and 7 of Table 2) and (b) the curved sections (sections 2 and 6). The histograms contain only those traces oriented within ±35° of the average trend; as a result, a small number of fault traces from the locked straight sections and a somewhat larger number of traces from the curved sections are omitted from the figures.

ern locked section, could develop in that time. In contrast (and in common with the previous hypothesis), the bending in the southern curved section may be reinforced by offsets on the Garlock and White Wolf faults (Crowell, 1979, p. 300).

Comparison of San Andreas and Experimental Fault Patterns

This study of recently active breaks of the San Andreas fault zone has revealed some distinctive features to compare with our experimental results. The segments of the curved and locked straight sections, described above, can be distinguished on the basis of their internal as well as external geometry, in that the curved sections have a lower proportion of parallel faults and a lower ratio of westward to northward traces than do the locked straight sections. Because of the many differences between the straight and curved sections, fault traces within the creeping section will be compared only to those in the locked straight sections. Two differences were found. First, the creeping section has a general lack of northward traces making large, positive angles to the strike of the fault zone; second, the creeping segments have more westward than northward traces, whereas the opposite relation is true for the locked straight segments.

The relationships between the San Andreas fault traces and the secondary shears of experimental studies are illustrated in Figure 1. The Y shears of laboratory faults correspond to the parallel breaks of the San Andreas, the R shears to northward-oriented San Andreas traces, and the P shears to westward-oriented traces. In our laboratory samples, the R and P shears make angles of at most ±35° to the boundaries of the gouge layer (Moore and others, 1986, 1988). All of the northward and westward traces of the creeping section fall within this range; the largest-angle traces in the locked sections do not, but the length of such traces compared to the total length of recent breaks is only about 1%. The ratios of westward to northward traces calculated for the locked sections in Table 3 are therefore not strictly analogous to P/R ratios, but imposing a 35° limit would change the values by at most 0.03 (see Moore and Byerlee, 1989, Table 5, p. 57). The relative abundances of R, Y, and P traces in the locked segments are similar to those measured by Keller and others (1982) along the southern San Andreas near Indio Hills.

In most respects, the San Andreas fault patterns closely correspond to those observed in our laboratory samples of fault gouge. The general absence of northward traces with angles greater than +15° from the creeping section and their presence in the locked straight sections is consistent with our measurements of lower Riedel angles in the stably sliding samples than in the stick-slip samples of fault gouge (Moore and others, 1989). The transition to purely stick-slip behavior for most of the gouge materials tested is associated with an increase in the maximum Riedel angle to 15° or greater. The differences in maturity suggested by the general segment characteristics of the curved and straight locked sections can also be extended to their internal fault patterns. The relatively low proportions of parallel traces and high proportions of northward traces in the curved sections can be correlated with the early stages of laboratory fault zone development in which R shears predominate. The higher proportions of parallel traces and lower proportions of northward traces in the locked straight sections reflect the increasing prominence of Y and, to a lesser extent, P shears in laboratory samples as displacement continues. Only the predominance of westward over northward traces in the creeping section is not immediately identifiable among the experimental results, because in most samples the P shears are subsidiary to the R shears. Even here, however, some correlation is present.

Because our earlier textural studies were concentrated on the R and Y shears, the many samples of illite gouge described by Moore and others (1989) were re-examined for P-shear development. Only 6 samples out of more than 100 contain P shears that equal or surpass the R shears in abundance. The six samples typically contain relatively wide secondary shears and a strongly developed planar fabric in between, making the overall textural development one of only moderately localized shear. They also have maximum Riedel angles of 14° or less, consistent with the truncated histogram of the creeping section (Fig. 8a). Lastly, the sliding behavior of the six samples ranges from stable slip to stick-slip with small stress drops, which also corresponds to the range from aseismic and episodic creep to earthquakes of small to moderate size observed in the creeping section (Burford and others, 1973; Wesson and others, 1973; Bakun and others, 1980).

Quality of Correlations

Before discussing the significance of the correlations between the natural and laboratory fault patterns, the level of confidence to be accorded them needs to be considered. Possible concerns include the quality of the San Andreas data and the extent to which laboratory and natural faults are comparable. Although these topics are discussed extensively in Moore and Byerlee (1989), the most important considerations are presented here.

Despite the general guidelines set down for the group of maps studied, each geologist involved in the project may have mapped the recent breaks differently. Segments of the creeping section have similar faulting patterns, however, even though they are on two maps prepared by different geologists. The distinctive characteristics of the creeping section, therefore, are not an artifact of one geologist's mapping procedure. In the same way, the special characteristics of the curved sections are in two maps, and at least short stretches of the locked straight sections are contained in five of the six maps.

The quality of the map data was investigated further by comparing the map of Davis and Duebendorfer (1987) with segments E-10a to E-15 from Vedder and Wallace (1970). The styles of the two maps differ somewhat; principally, several of the longer, continuous fault traces in Vedder and Wallace (1970) are represented as sets of short, *en echelon* traces by Davis and Duebendorfer (1987). Davis and Duebendorfer also identified thrust faults that, along with traces that were designated as being older and possibly inactive, were not included in the measurements. Use of the newer map leads to the division of segment E-13 into two segments and the shifting of a few segment boundaries by a maximum of 800 m. The combined histogram of fault length and orientation obtained from Davis and Duebendorfer (1987) is also somewhat flattened compared to the one for the corresponding segments from Vedder and Wallace (1970), but the range of orientations of the northward traces and the proportions of parallel, westward, and northward traces obtained from the two maps are nearly the same. Use of either map would lead to the same conclusions about fault patterns in the western Big Bend area.

Another potential source of error is the choice of segment orientations. For example, a modest change in the average trend can greatly affect the total lengths assigned to parallel, northward, and westward traces in a given segment. If the average trend of each creeping segment were shifted 1° to the west, and the average trend of each of the locked segments were shifted 1° to the north, then much of the difference between the lengths of westward and northward traces in the locked and creeping portions of the fault would be removed. Such a pronounced bias in the determination of the average trends seems unlikely, because for many of the segments, particularly the longer ones of the straight sections, the tolerance in the positioning of the average trend line is considerably less than 1°. The greatest tolerance would be found in the relatively short and wide segments of the curved sections, the fault patterns of which were not included in the comparison with the creeping section.

Consideration of the stepovers between adjoining, recently active breaks supports the suggestion of a difference in the distributions of westward and northward traces between the creeping and locked straight sections. A group of westward (P) traces in an *en echelon* array along the San Andreas would be separated by right stepovers, whereas a group of northward (R) *en echelon* traces would be separated by left stepovers (Fig. 1). If the histograms of Figures 8a and 9a are valid, then the creeping section should contain more right than left stepovers between the recent breaks, and the locked straight sections should contain more left than right stepovers. Stepover counts for these four sections were made by following a principal slip path along the length of each section. The numbers vary, depending on the treatment of equivocal areas, and a range of stepover counts was obtained for each section. The ratio of right to left stepovers for the creeping section ranges from about 3:2 to nearly 2:1; in contrast, the ratios for the locked sections are all less than 1:1, ranging from less than 1:2 for the southern locked section to 3:4 to 7:8 for the central locked section. These results are consistent with the distributions of recent breaks shown in Figures 8a and 9a and calculated in Table 3. This correspondence is important, because the stepover ratios are independent of the choice of average trend lines and the subdivision of the recent breaks for orientation measurements.

An additional consideration is the applicability of our experiments to natural faults. Because the laboratory experiments were conducted at high pressures, comparison of the experimental textures with surficial fault patterns is only appropriate is the surface structures are representative of those found at deeper levels. This question cannot be answered at present, because we have very little knowledge of the deep structure of faults. Many workers have assumed that faulting patterns are simpler at depth, and in keeping with this idea, most shear box and sand box experiments, as well as the intact-rock experiments of Bartlett and others (1981), have been conducted with a single, straight, narrow fault at the base of the samples. Sharp (1979) envisioned a simple but possibly very wide fault zone at depth. In contrast, examination of faults exposed in deep mines has shown that the fault patterns remain complex to at least that level (Wallace and Morris, 1986). The ore-bearing faults that were studied by Wallace and Morris may have originally formed at depths to about 5 km. Some of the major surface irregularities in the San Andreas and Calaveras fault zones have been identified at depth by means of detailed microseismic studies (Eaton and others, 1970; Bakun and others, 1980; Reasenberg and Ellsworth, 1982). In their fractal analyses of the San Andreas fault, both Aviles and others (1987) and Okubo and Aki (1987) also supported the suggestion that the mapped surface irregularities extend to deeper levels within the seismogenic zone.

Significance of Results

If the correlations between the experimental and natural fault patterns are valid, then knowledge of the controls on textural development in the experiments will be important to understand the behavior of faults in nature. At present, however, neither the variations in Riedel angle nor the relative proportions of R and P shears can be explained in terms of Coulomb-Mohr theory. The orientations of the R shears in the laboratory samples should seemingly be related to their function as Coulomb shears, yet the shear orientations cannot be related in a simple way to Coulomb theory. Briefly, the angle that the R shears make with the boundary of the fault zone should equal half the angle of internal friction of the material being tested (for example, Mandl and others, 1977). Given the experimental fault zone evolution described previously, and given no subsequent passive rotation of the shears, the largest-angle R shears should be the ones that obey the Coulomb equation. For the illite-rich gouge examined by Moore and others (1989), however, the angles of internal friction calculated from plots of normal versus shear stress do not agree with those obtained from the maximum Riedel angles. Use of an average rather than the maximum Riedel angle for the calculations produces an even worse fit for most of the samples.

Our six samples of illite gouge containing many P shears are identical with respect to sliding behavior, degree of localization of shear, and Riedel angles to many other samples that contain predominantly R shears. The creeping section, therefore, appears to be correlated with the exceptional rather than the normal samples. The experimental samples containing many P shears were produced under a variety of experimental conditions, and there is no obvious explanation for the development of their atypical fault patterns. As described previously, from models of the evolution of strike-slip faults based on Coulomb-Mohr theory, P shears should be secondary structures and generally subordinate to R shears in their occurrence. The *en echelon* arrays of westward (P) traces in the San Andreas fault zone figured in Wallace (1973), however, appear to be primary rather than secondary arrays, because they form the principal (or only) mapped traces in those parts of the fault. Bartlett and others (1981) also reported the possibly concurrent rather than sequential development of R and P shears in laboratory strike-slip fault zones that they generated in initially intact layers of limestone. Similarly, in our samples of illite gouge containing many P shears, those shears appear to be primary structures that are connected by secondary R shears. The formation of primary P shears is not explainable by Coulomb-Mohr theory (Bartlett and others, 1981; Gamond, 1987). Some natural, *en echelon* P faults have been suggested to form where dilation of the fault zone is possible (Vialon, 1979; Gamond, 1983), but dilation cannot be invoked to explain P-shear development in our samples, at least, because the experiments were run under high effective pressures, for which dilation would be considerably suppressed.

CONCLUDING REMARKS

Two differences have been found between the fault patterns of the creeping and locked sections of the San Andreas. The fault geometry of the locked segments is readily correlated with that of laboratory samples characterized by stick-slip displacement. On the other hand, the geometry of recent breaks of the creeping segments corresponds best to a small number of samples with sliding behavior that is transitional between stable and stick-slip. Future experimental studies conducted to understand fault creep may best be concentrated, therefore, in the region of transitional sliding behavior rather than that of purely stable slip, under conditions that favor the development of P shears. If the special features of the creeping section can eventually be related to its sliding behavior, then the patterns of recent breaks will provide a useful tool for the evaluation of seismic potential. Because of this, further work must corroborate these results and identify the origin of the fault patterns.

ACKNOWLEDGMENTS

This work has been reviewed, at various stages, by A. Aydin, R. Bilham, M. Blanpied, R. Brown, E. Duebendorfer, R. Sharp, A. G. Sylvester, R. Wallace, and M. L. Zoback.

REFERENCES CITED

Atwater, T., 1970, Implications of plate tectonics for the Cenozoic tectonic evolution of western North America: Geological Society of America Bulletin, v. 81, p. 3513–3536.

Atwater, T., and Molnar, P., 1973, Relative motion of the Pacific and North American plates deduced from sea-floor spreading in the Atlantic, Indian, and South Pacific Oceans, *in* Kovach, R. L., and Nur, A., eds., Proceedings of the Conference on Tectonic Problems of the San Andreas Fault System: Stanford University Publications in Geological Sciences, v. 13, p. 136–148.

Aviles, C. A., Scholz, C. H., and Boatwright, J., 1987, Fractal analysis applied to characteristic segments of the San Andreas fault: Journal of Geophysical Research, v. 92, p. 331–344.

Aydin, A., and Page, B. M., 1984, Diverse Pliocene-Quaternary tectonics in a transform environment, San Francisco Bay region, California: Geological Society of America Bulletin, v. 95, p. 1303–1317.

Bakun, W. H., Stewart, R. M., Bufe, C. G., and Marks, S. M., 1980, Implication of seismicity for failure of a section of the San Andreas fault: Seismological Society of America Bulletin, v. 70, p. 185–201.

Barka, A. A., and Kadinsky-Cade, K., 1988, Strike-slip fault geometry in Turkey and its influence on earthquake activity: Tectonics, v. 7, p. 663–684.

Bartlett, W. L., Friedman, M., and Logan, J. M., 1981, Experimental folding and faulting of rocks under confining pressure. Part IX. Wrench faults in limestone layers: Tectonophysics, v. 79, p. 255–277.

Biddle, K. T., and Christie-Blick, N., 1985, Glossary—Strike-slip deformation, basin formation, and sedimentation, *in* Biddle, K. T., and Christie-Blick, N., eds., Strike-slip deformation, basin formation, and deformation: Society of Economic Paleontologists and Mineralogists Special Publication 37, p. 375–386.

Bilham, R., and King, G., 1989, Slip distribution on oblique segments of the San Andreas fault, California: Observations and theory, *in* Schwartz, D. P., and Sibson, R. H., eds., Fault segmentation and controls of rupture initiation and termination: U.S. Geological Survey Open-File Report 89-315, p. 80–93.

Bilham, R., and Williams, P., 1985, Sawtooth segmentation and deformation processes on the southern San Andreas fault, California: Geophysical Research Letters, v. 12, p. 557–560.

Bohannon, R. G., and Howell, D. G., 1982, Kinematic evolution of the junction of the San Andreas, Garlock, and Big Pine faults, California: Geology, v. 10, p. 358–363.

Brown, R. D., Jr., 1970, Map showing recently active breaks along the San Andreas and related faults between the northern Gabilan Range and Cholame Valley, California: U.S. Geological Survey Miscellaneous Geological Investigations Map I-575, scale 1:62,500.

——— 1972, Active faults, probable active faults, and associated fracture zones, San Mateo County, California: U.S. Geological Survey Miscellaneous Field Studies Map MF-355, scale 1:62,500.

Brown, R. D., Jr., and Wolfe, E. D., 1972, Map showing recently active breaks along the San Andreas fault between Point Delgada and Bolinas Bay, California: U.S. Geological Survey Miscellaneous Geological Investigations Map I-692, scale 1:24,000.

Burford, R. O., Allen, S. S., Lamson, R. J., and Goodreau, D. D., 1973, Accelerated fault creep along the central San Andreas fault after moderate earthquakes during 1971–1973, *in* Kovach, R. L., and Nur, A., eds., Proceedings of the Conference on Tectonic Problems of the San Andreas Fault System: Stanford University Publications in Geological Sciences, v. 13, p. 268–274.

Byerlee, J., Mjachkin, V., Summers, R., and Voevoda, O., 1978, Structures developed in fault gouge during stable sliding and stick-slip: Tectonophysics, v. 44, p. 161–171.

Clark, M. M., 1984, Map showing recently active breaks of the San Andreas fault and associated faults between Salton Sea and Whitewater River–Mission Creek, California: U.S. Geological Survey Miscellaneous Geological Investigations Map I-1483, scale 1:24,000.

Cloos, H., 1928, Experimente zur inneren Tektonik: Zentralblatt von Mineralogie, Geologie, und Paleontologie, Abt. B., p. 609–671.

Crowell, J. C., 1974a, Sedimentation along the San Andreas fault, California, *in* Dott, R. H., Jr., and Shaver, R. H., eds., Modern and ancient geosynclinal sedimentation: Society of Economic Paleontologists and Mineralogists Special Publication 19, p. 292–303.

——— 1974b, Origin of late Cenozoic basins in southern California, *in* Dickinson, W. R., ed., Tectonics and sedimentation: Society of Economic Paleontologists and Mineralogists Special Publication 22, p. 190–204.

——— 1979, The San Andreas fault system through time: Geological Society of London Journal, v. 136, p. 293–302.

Davis, G. A., and Burchfiel, B. C., 1973, Garlock fault: An intracontinental transform structure, southern California: Geological Society of America Bulletin, v. 84, p. 1407–1422.

Davis, T. L., and Duebendorfer, E. M., 1987, Strip map of the western Big Bend segment of the San Andreas fault: Geological Society of America Map and Chart Series Map MC-60, scale 1:31,682.

Dickinson, W. R., 1966, Structural relationships of San Andreas fault system, Cholame Valley and Castle Mountain Range, California: Geological Society of America Bulletin, v. 77, p. 707–726.

Eaton, J. P., O'Neill, M. E., and Murdock, J. N., 1970, Aftershocks of the 1966 Parkfield-Cholame, California, earthquake: A detailed study: Seismological Society of America Bulletin, v. 60, p. 1151–1197.

Gamond, J. F., 1983, Displacement features associated with fault zones: A comparison between observed examples and experimental models: Journal of Structural Geology, v. 5, p. 33–45.

——— 1987, Bridge structures as sense of displacement criteria in brittle fault zones: Journal of Structural Geology, v. 9, p. 609–620.

Herd, D. G., 1977, Map of Quaternary faulting along the Hayward and Calaveras fault zones; Niles and Milpitas 7½' quadrangles, California: U.S. Geological Survey Open-File Map 77-645, scale 1:24,000.

——— 1978, Map of Quaternary faulting along the northern Hayward fault zone: U.S. Geological Survey Open-File Report 78-308, scale 1:24,000.

Hope, R. A., 1969, Map showing recently active breaks along the San Andreas and related faults between Cajon Pass and Salton Sea, California: U.S. Geological Survey Open-File Map, scale 1:24,000.

Keller, E. A., Bonkowski, M. S., Korsch, R. J., and Shlemon, R. J., 1982, Tectonic geomorphology of the San Andreas fault zone in the southern Indio Hills, Coachella Valley, California: Geological Society of America Bulletin, v. 93, p. 45–56.

Knuepfer, P.L.K., 1989, Implications of the characteristics of end-points of historical surface fault ruptures for the nature of fault segmentation, *in* Schwartz, D. P., and Sibson, R. H., eds., Fault segmentation and controls of rupture initiation and termination: U.S. Geological Survey Open-File Report 89-315, p. 193–228.

Lindh, A. G., and Boore, D. M., 1981, Control of rupture by fault geometry during the 1966 Parkfield earthquake: Seismological Society of America Bulletin, v. 71, p. 95–116.

Logan, J. M., and Rauenzahn, K. A., 1987, Frictional dependence of gouge mixtures of quartz and montmorillonite on velocity, composition, and fabric: Tectonophysics, v. 144, p. 87–108.

Logan, J. M., Friedman, M., Higgs, N., Dengo, C., and Shimamoto, T., 1979, Experimental studies of simulated gouge and their application to studies of natural fault zones, *in* Proceedings of Conference VIII: Analysis of actual fault zones in bedrock: U.S. Geological Survey Open-File Report 79-1239, p. 305–343.

Logan, J. M., Higgs, N. G., and Friedman, M., 1981, Laboratory studies on natural gouge from U.S. Geological Survey Dry Lake Valley No. 1 well, San Andreas fault zone, *in* Carter, N. L., Friedman, M., Logan, J. M., and Stearns, D. W., eds., Mechanical behavior of crustal rocks: American Geophysical Union Monograph 24, p. 121–134.

Loomis, D. P., and Burbank, D. W., 1988, The stratigraphic evolution of the El Paso basin, southern California: Implications for the Miocene development of the Garlock fault and uplift of the Sierra Nevada: Geological Society of America Bulletin, v. 100, p. 12–28.

Mandl, G., 1988, Mechanics of tectonic faulting: New York, Elsevier, 407 p.

Mandl, G., de Jong, L.N.J., and Maltha, A., 1977, Shear zones in granular material: An experimental study of their structure and mechanical genesis: Rock Mechanics, v. 9, p. 95–144.

Moore, D. E., and Byerlee, J., 1989, Geometry of recently active breaks along the San Andreas fault, California: U.S. Geological Survey Open-File Report 89-347, 72 p.

Moore, D. E., Summers, R., and Byerlee, J. D., 1983, Strengths of clay and non-clay fault gouges at elevated temperatures and pressures: 24th U.S. Symposium on Rock Mechanics, Proceedings, p. 489–500.

——— 1986a, The effects of sliding velocity on the frictional and physical properties of heated fault gouge, *in* Wang, C.-Y., ed., Internal structure of fault zones: Pure and Applied Geophysics, v. 124, p. 31–52.

——— 1986b, Strength measurements of heated illite gouge at low and high pore pressures: U.S. Geological Survey Open-File Report 86-578, 28 p.

——— 1988, Relationship between textures and sliding motion of experimentally deformed fault gouge: Application to fault zone behavior: 29th U.S. Symposium on Rock Mechanics, Proceedings, p. 103–110.

——— 1989, Sliding behavior and deformation textures of heated illite gouge: Journal of Structural Geology, v. 11, p. 329–342.

Morgenstern, N. R., and Tchalenko, J. S., 1967, Microscopic structures in kaolin subjected to direct shear: Géotechnique, v. 17, p. 309–328.

Naylor, M. A., Mandl, G., and Sijpesteijn, C.H.K., 1986, Fault geometries in basement-induced wrench faulting under different initial stress states: Journal of Structural Geology, v. 8, p. 737–752.

Okubo, P. G., and Aki, K., 1987, Fractal geometry in the San Andreas fault system: Journal of Geophysical Research, v. 92, p. 345–355.

Page, B. M., 1982, The Calaveras fault zone of California—An active plate boundary element, *in* Hart, E. W., Hirschfeld, S. E., and Schulz, S. S., eds., Proceedings of the Conference on Earthquake Hazards in the Eastern San Francisco Bay Area: California Division of Mines and Geology Special Publication 62, p. 175–184.

Radbruch-Hall, D. H., 1974, Map showing recently active breaks along the Hayward fault zone and the southern part of the Calaveras fault zone, California: U.S. Geological Survey Miscellaneous Geological Investigations Map I-813, scale 1:24,000.

Reasenberg, P., and Ellsworth, W. L., 1982, Aftershocks of the Coyote Lake, California earthquake of August 6, 1979: A detailed study: Journal of Geophysical Research, v. 87, p. 10637–10655.

Riedel, W., 1929, Zur Mechanik geologischer Brucherscheinungen: Zentralblatt von Mineralogie, Geologie, und Paleontologie, Abt. B, p. 354–368.

Rodgers, D. A., 1980, Analysis of pull-apart basin development produced by en echelon strike-slip faults, *in* Ballance, P. F., ed., Sedimentation in oblique-slip mobile zones: International Association of Sedimentology Special Publication 4, p. 27–41.

Ross, D. C., 1969, Map showing recently active breaks along the San Andreas fault between Tejon Pass and Cajon Pass, southern California: U.S. Geological Survey Miscellaneous Investigations Series Map I-533, scale 1:24,000.

Rutter, E. H., Maddock, R. H., Hall, S. H., and White, S. H., 1986, Comparative microstructures of natural and experimentally produced clay-bearing fault gouges, *in* Wang, C.-Y., ed., Internal structure of fault zones: Pure and Applied Geophysics, v. 124, p. 3–30.

Sarna-Wojcicki, A. M., Pampeyan, E. H., and Hall, N. T., 1975, Map showing recently active breaks along the San Andreas fault between the central Santa Cruz Mountains and the northern Gabilan Range, California: U.S. Geological Survey Miscellaneous Field Studies Map MF-650, scale 1:24,000.

Schwartz, D. P., and Coppersmith, K. J., 1984, Fault behavior and characteristic earthquakes: Examples from the Wasatch and San Andreas fault zones: Journal of Geophysical Research, v. 89, p. 5681–5698.

Segall, P., and Pollard, D. D., 1980, Mechanics of discontinuous faults: Journal of Geophysical Research, v. 85, p. 4337–4350.

Sharp, R. V., 1971, Map showing recently active breaks along the San Jacinto fault zone between the San Bernardino area and Borrego Valley, California: U.S. Geological Survey Miscellaneous Geological Investigations Map I-675, scale 1:24,000.

——— 1979, Implications of surficial strike-slip fault patterns for simplification and widening with depth, *in* Proceedings of Conference VIII: Analysis of actual fault zones in bedrock: U.S. Geological Survey Open-File Report 79-1239, p. 66–78.

Shedlock, K. M., Brocher, T. M., and Harding, S. T., 1990, Shallow structure and deformation along the San Andreas fault in Cholame Valley, California, based on high-resolution reflection profiling: Journal of Geophysical Research, v. 95, p. 5003–5020.

Sibson, R. H., 1985, Stopping of earthquake ruptures at dilational fault jogs: Nature, v. 316, p. 248–251.

——— 1986, Rupture interaction with fault jogs: American Geophysical Union Geophysical Monograph 37 (Maurice Ewing Volume 6), p. 157–167.

Sims, J. D., 1988, Geologic map of the San Andreas fault zone in the Cholame Valley and Cholame Hills quadrangles, San Luis Obispo and Monterey Counties, California: U.S. Geological Survey Miscellaneous Field Studies Map MF-1995, scale 1:24,000.

Summers, R., and Byerlee, J., 1977, Summary of results of frictional sliding studies, at confining pressures up to 6.98 kb, in selected rock materials: U.S. Geological Survey Open-File Report 77-142, 129 p.

Sylvester, A. G., 1988, Strike-slip faults: Geological Society of America Bulletin, v. 100, p. 1666–1703.

Tchalenko, J. S., 1970, Similarities between shear zones of different magnitudes: Geological Society of America Bulletin, v. 81, p. 1625–1640.

Vedder, J. G., and Wallace, R. E., 1970, Map showing recently active breaks along the San Andreas and related faults between Cholame Valley and Tejon Pass, California: U.S. Geological Survey Miscellaneous Geological Investigations Map I-574, scale 1:24,000.

Vialon, P., 1979, Les déformations continues-discontinues des roches anisotropes: Eclogae Geologicae Helvetiae, v. 72, p. 531–549.

Wallace, R. E., 1973, Surface fracture patterns along the San Andreas fault, *in* Kovach, R. L., and Nur, A., eds., Proceedings of the Conference on Tectonic Problems of the San Andreas Fault System: Stanford University Publications in Geological Science, v. 13, p. 248–250.

Wallace, R. E., and Morris, H. T., 1986, Characteristics of faults and shear zones in deep mines, *in* Wang, C.-Y., ed., Internal structure of fault zones: Pure and Applied Geophysics, v. 124, p. 107–125.

Weaver, C. S., and Hill, D. P., 1978, Earthquake swarms and local crustal spreading along major strike-slip faults in California: Pure and Applied Geophysics, v. 117, p. 51–64.

Wesnousky, S. G., 1988, Seismological and structural evolution of strike-slip faults: Nature, v. 335, p. 340–343.

Wesson, R. L., Burford, R. O., and Ellsworth, W. L., 1973, Relationship between seismicity, fault creep, and crustal loading along the central San Andreas fault, *in* Kovach, R. L., and Nur, A., eds., Proceedings of the Conference on Tectonic Problems of the San Andreas Fault System: Stanford University Publications in Geological Science, v. 13, p. 303–321.

Manuscript Received by the Society November 20, 1989
Revised Manuscript Received September 5, 1990
Manuscript Accepted September 11, 1990